International Journal of Applied Earth Observation and Geoinformation 21 (2013) 311–325

Contents lists available at SciVerse ScienceDirect

International Journal of Applied Earth Observation and Geoinformation

journal homepage: www.elsevier.com/locate/jag

Diurnal rainfall variability over the Upper Blue Nile Basin: A remote sensing based approach

Tom Rientjes[a,*], Alemseged Tamiru Haile[b], Ayele Almaw Fenta[c]

[a] Department of Water Resources, Faculty of Geo-information Science and Earth Observation (ITC), University of Twente, P.O. Box 6, 7500AA Enschede, The Netherlands
[b] African Climate Policy Center, United Nations Economic Commission for Africa, P.O. Box 3001, Addis Ababa, Ethiopia
[c] Department of Land Resources Management and Environmental Protection, College of Dryland Agriculture and Natural Resources, Mekelle University, P.O. Box 231, Mekelle, Tigray, Ethiopia

ARTICLE INFO

Article history:
Received 20 February 2012
Accepted 12 July 2012

Keywords:
Diurnal rainfall
TRMM TMI
TRMM PR
Upper Blue Nile

ABSTRACT

In this study we aim to assess the diurnal cycle of rainfall across the Upper Blue Nile (UBN) basin using satellite observations from Tropical Rainfall Measuring Mission (TRMM). Seven years (2002–2008) of Precipitation Radar (PR) and TRMM Microwave Imager (TMI) data are used and analyses are based on GIS operations and simple statistical techniques. Observations from PR and TMI reveal that over most parts of the basin area, the rainfall occurrence and conditional mean rain rate are highest between mid- and late-afternoon (15:00–18:00 LST). Exceptions to this are the south-west and south-eastern parts of the basin area and the Lake Tana basin where midnight and early morning maxima are observed. Along the Blue Nile River gorge the rainfall occurrence and the conditional mean rain rate are highest during the night (20:00–23:00 LST). Orographic effects by large scale variation of topography, elevation and the presence of the UBN river gorge were assessed taking two transects across the basin. Along transects from north to south and from east to west results indicate increased rainfall with increase of elevation whereas areas on the windward side of the high mountain ranges receive higher amount of rainfall than areas on the leeward side. As such, mountain ranges and elevation affect the rainfall distribution resulting in rain shadow effect in the north-eastern parts of Choke-mountain and the ridges in the north-east of the basin. Moreover, a direct relation between rainfall occurrence and elevation is observed specifically for 17:00–18:00 LST. Further, results indicate that the rainfall distribution in the deeply incised and wide river gorge is affected with relatively low rainfall occurrence and low mean rainfall rates in the gorge areas. Seasonal mean rainfall depth is highest in the south-west area and central highlands of the basin while areas in the north, north-east and along the Blue Nile gorge receive the least amount of rainfall. Statistical results of this work show that the diurnal cycle of rainfall occurrence from TRMM estimates show significant correlation with the ground observations at 95% confidence level. In the UBN basin, the PR conditional mean rain rate estimates are closer to the ground observations than the TMI. Analysis on mean wet season rainfall amount indicates that PR generally underestimates and TMI overestimates the ground observed rainfall.

1. Introduction

A large number of studies report on assessments of time–space variability of rainfall characteristics such as rainfall rate, depth and occurrence. For applications in hydro-meteorology and operational water management, assessments commonly aim at daily, monthly or larger time scales and spatial domains that match or exceed the regional scale (>500 km^2). Studies that exclusively focus on rainfall variability at smaller time scales such as the sub-daily scale or hourly time scale to represent the diurnal cycle are limited. Poor data availability often constrains such assessments particularly when rain gauge networks have low density and when observation networks have not been designed following certain criteria (e.g. Muthuwatta et al., 2010). The latter aspects often apply to less developed countries where financial resources are limited and where stations are located close to urban areas because of easy site accessibility. Further, most stations are rainfall collector stations for which observations are taken once per day. In contrast to the poor rainfall observation, the importance to observe rainfall over large spatial domains at sub-daily time resolution is eminent for adequate water management in particular for regionalisation studies (see Wale et al., 2009; Deckers et al., 2010; Rientjes et al., 2011b), advanced hydrological modelling (Zhang et al., 2005; Fenicia et al., 2005; de Vos and Rientjes, 2008; de Vos et al., 2010), flood

* Corresponding author.
E-mail addresses: t.h.m.rientjes@utwente.nl, rientjes@itc.nl (T. Rientjes).

0303-2434/$ – see front matter © 2012 Elsevier B.V. All rights reserved.
http://dx.doi.org/10.1016/j.jag.2012.07.009

modelling (see Tarekegn et al., 2010), climate and land use change impact assessments (Abdo et al., 2009; Rientjes et al., 2011a) but also since rainfall in the tropics plays an important role in the global hydrological cycle with two-third of the global rainfall that falls in the tropical regions between 30°N and 30°S.

For the Upper Blue Nile (UBN) basin in Ethiopia Conway (2000) indicated that seasonal rainfall is highly variable when analysing monthly rainfall data. In the same work it is described that there are three mechanisms that influence the rainfall characteristics of Ethiopia. These are the Inter Tropical Convergence Zone (ITCZ) that drives the summer monsoon during the wet season, the Saharan anticyclone that generates dry warm north-easterly winds during the dry season, and the Arabian heights that produce thermal lows during the inter seasonal periods. Aspects of large scale wind circulation over the source region of the Nile were studied in Camberlin (1997) and results indicated that during the rainy season a general south-westerly monsoon flow can be noticed while in eastern Africa as a whole, wind flows are distinctly affected by topographic features. Further, in Camberlin (2009) it is described that topography is the most important factor that modifies the general circulation pattern since mountain ranges generate local wind circulation patterns that result in specific local climate conditions. Also large water bodies such as lakes tend to develop their own local circulation patterns in the form of lake breezes that are induced by differences in diurnal temperature variations of the lake as compared to the surrounding land areas. Day-time breezes diverge from lakes to the warmer surrounding land and night-time land breezes converge to the warmer middle part of the lakes affecting spatial and temporal distribution of rainfall (see Haile et al., 2009, 2012b).

An alternative approach to the use of a ground based observation network is to observe rainfall by satellites that may be geo-stationary or in orbit. Satellites have the potential to systematically observe information over large spatial domains with specific revisit interval. Therefore a time series of rainfall satellite images provides the opportunity to assess the diurnal cycle of selected rainfall properties in poorly gauged areas such as the Upper Blue Nile River basin in Ethiopia, East Africa. To enhance our understanding of tropical rainfall, the TRMM satellite was launched in 1997. The two main sensors of TRMM are the Precipitation Radar (PR) and TRMM Microwave Imager (TMI) that rely on active and passive microwave remote sensing, respectively. Simpson et al. (1988) describe that one of the priority science questions that led to the launch of the TRMM satellite was "What is the diurnal cycle of tropical rainfall and how does it vary in space?" TRMM is a non-Sun synchronous orbiting satellite and thus revisits certain areas at different local times of a day. In practice, any specific geographic location for any specific local time is revisited only once in 46 days that as such is a major constraint for detailed analysis at sub-daily time scales (see Bell and Reid, 1993). The fact, however, that regions are visited at different local time is the premise that assessments of the diurnal cycle of rainfall are possible using TRMM observations. As such, in the present study we exclusively focus on assessing the diurnal cycle of rainfall by TRMM over the UBN basin.

A number of studies report on the assessment of diurnal cycle of rainfall by TRMM. Negri et al. (2002) used three years of data of TRMM PR and TMI to describe the rainfall diurnal cycle for tropical areas as large as $5^\circ \times 5^\circ$ and $10^\circ \times 25^\circ$ ($1^\circ \approx 111$ km). Results in the study indicated that TMI and PR observations exhibit some differences in terms of magnitude and phase of both rain rate and frequency and that, over land, TMI estimates of rain rate tend to be higher than PR estimates. Bowman et al. (2005) also reported that TMI rain rates are higher than PR rain rates over land surfaces and tropical oceans. Also, TMI results indicate larger diurnal variation whereas differences in phase between the diurnal cycles of rain rates by the sensors were not consistent. Hirose et al. (2008) aggregated 8 years of TRMM data over a $1^\circ \times 1^\circ$ grid box and found that TMI rain rates and frequencies were significantly lower than PR counterparts over western and central Tibet. In addition, rainfall amount and frequency over areas in eastern Tibet showed morning to early-afternoon peaks for TMI data and evening peaks for PR data. Kishtawal and Krishnamurti (2001) studied the diurnal cycle of rainfall using five months of TMI observations for the entire Taiwan. Results were validated by ground observations and showed that the diurnal patterns of TMI rainfall rates reasonably matched to ground observations although TMI consistently indicated higher rain rates. Ikai and Nakamura (2003) on the other hand reported that PR-rain rates are higher than TMI-rain rates in mountainous regions over land such as the Rocky-mountains, the Andes, and the Himalayas. The authors spatially averaged the data over an area of size $5^\circ \times 5^\circ$ to overcome sample size limitations. Using 6 years of TRMM data, Yamamoto et al. (2008) found systematic shifts in peak time relative to the diurnal cycles derived from the two sensors over western North America, the Tibetan Plateau, and oceanic regions such as the Gulf of Mexico. The systematic shifts are particular to regions with high convective frequency and large rain event depth, and large amplitude of diurnal variation. Using eight years of TMI and PR estimates, Ji (2006) made a comparison of mean hourly rainfall and diurnal cycles between TRMM satellite and ground observations over Florida (USA) and sites in Darwin (Australia). It was reported that the diurnal cycles from PR and TMI estimates are comparable to the gauge observations with small amplitude differences between PR and gauge data while TMI observations showed larger amplitudes. Furuzawa and Nakamura (2005) report that over land surface, PR rain rate estimates better matched ground observations compared to TMI. They attributed this to PR's superior vertical and horizontal resolution that allows PR to observe smaller scale precipitation features that cannot be unambiguously resolved by the TMI.

The aim of this study is to assess the rainfall diurnal cycle for the UBN basin by TRMM PR and TRMM TMI observations. For such assessment diurnal cycles of rainfall occurrence and rainfall rate are constructed and results of PR and TMI are compared and evaluated. We evaluate if large scale terrain relief by the UBN gorge, Choke-mountain and Lake Tana cause orographic effects with specific time–space variability. We use 7 years of data which provides a larger sample size than most of the aforementioned studies. Haile et al. (2009, 2011, 2012a), in detailed studies on rainfall variability in Lake Tana basin, indicated that rainfall properties are affected by a number of topographic and meteorological factors and signifies that accurate estimation is a major challenge in the UBN basin. This in particular for mountainous regions where in addition to the stochastic nature of rainfall, the rainfall pattern may be influenced by catchment orography.

In this study we selected the Precipitation Radar (PR) (2A25) and TRMM Microwave Imager (TMI) (2A12) products to assess the diurnal cycle for rainfall occurrence and mean rain rate and accumulated rainfall depth for the wet season months June, July, August, September (JJAS). For validation of the diurnal cycle estimates a comparison is made to ground observations. Effects of large scale topographic features such as Choke-mountain, the deep and wide gorge in the main stream of the UBN River and Lake Tana on the rainfall diurnal cycle properties of occurrence and rain rate are assessed by means of two transects that cross the basin area from north to south-east (NS) and from west to east (WE) directions. To broaden the TRMM performance assessment we compared the accumulated diurnal estimates of TRMM at daily base to gauged counterparts from some 9 collector stations.

Following Section 1, Section 2 presents the study area and discusses the available ground observations and satellite rainfall data. Section 3 discusses the methodology. Section 4 discusses the results of TRMM satellite sampling of the study area and the rainfall diurnal cycle in terms of rainfall occurrence and mean rain rate for

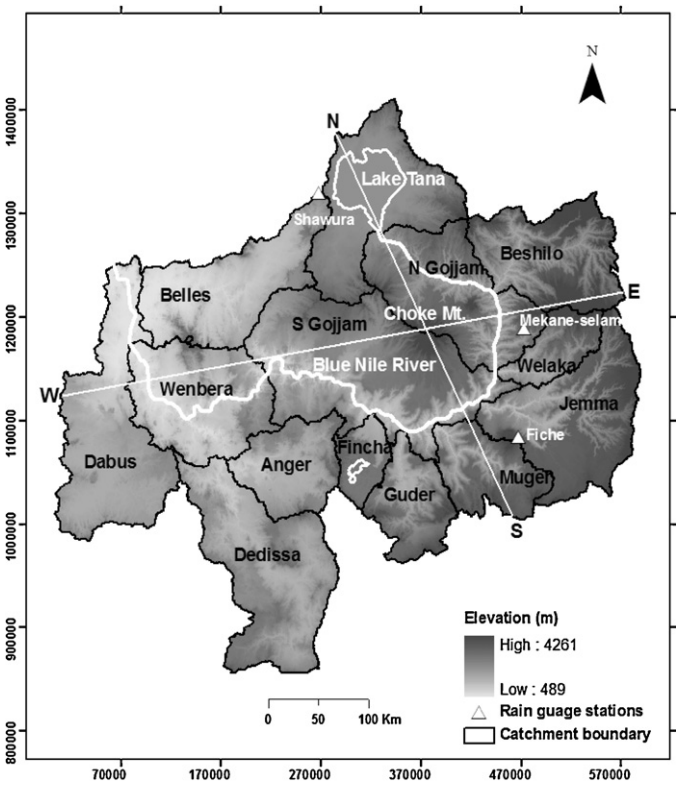

Fig. 1. DEM with sub-basins of the Upper Blue Nile Basin extracted from SRTM. Two transects from north to south-east (NS) and from west to east (WE), the main stream of the Upper Blue Nile (in white), Lake Tana and rain gauges are added (projection, UTM-zone 37N; datum, WGS1984; ellipsoid, WGS84).

conditional and unconditional mean rain rates. In the same section results of validation of PR and TMI diurnal cycle estimates and the spatial variability of rainfall are described. Also results on a comparison of daily estimates of PR and TMI and gauges observations are presented. Section 5 concludes on this study.

2. Study area and data

The Upper Blue Nile (UBN) basin is the source region of the Blue Nile River that drains large parts of the central and south-western Ethiopian Highlands. The UBN River (~800 km) runs from Lake Tana to the Sudanese border and merges with the White Nile River at Khartoum, Sudan. The river is characterised by its twisty route through the central Ethiopian Highlands and at some places the river is deeply incised with gorges as deep as 1500 m. More than 85% of the Nile River flows originate from the Ethiopian Highlands while the Blue Nile River contributes about 60% of the Nile River flow (see Sutcliffe and Parks, 1999; Conway, 2000).

The UBN basin is characterised by complex topography consisting of undulating terrain, high mountain ranges, deep and wide river gorges, a dense river network and flat grassland areas. Much of the highland areas have elevations above 1500 m above sea level with maximum of around 4200 m at Choke-mountain. The total drainage area of the basin is about 173,000 km^2 as extracted from a 90 m resolution Shuttle Radar Topography Mission (SRTM) Digital Elevation Model (DEM) (see Fig. 1). The area is located between 7°44′32″ to 12°45′19″ north latitude and 34°29′20″ to 39°48′17″ east longitude. The livelihood of the people in the basin is largely dependent on rain fed agriculture and small-scale irrigation.

2.1. Climate

The climate of the UBN basin varies from humid to semi-arid with a dry season from November to April. The months of October and May are transitional months from the wet season to the dry season and from the dry season to the wet season respectively. Conway (2000) describes that during the wet season in June–September approximately 70% of the annual rainfall is observed. UNESCO (2004) reports that annual rainfall across the basin is in the range of 1200–1600 mm with an increasing trend from north-east to south-west. Kim et al. (2008) describe that large scale topography strongly influences the climate and human activities although a detailed analysis is not presented. The same work reports that particularly during the wet season, rainfall is characterised by relatively high spatial variability.

2.2. Satellite observations

For this study we selected the Precipitation Radar (PR) (2A25) and TRMM Microwave Imager (TMI) (2A12) estimated surface rain (mm h^{-1}) products from the TRMM satellite that is a non-Sun synchronous orbiting satellite at an altitude of 402 km with inclination angle 35° and orbital period of 92 min. For the period 2002–2008 some 1100 PR images and 1600 Level-2 TMI images for the June, July, August, September (JJAS) wet season are collected. By this sample, the number of observation per pixel per Local Standard Time (LST) ranged from 8 to 20 for PR and from 37 to 50 for TMI with means of 13 and 43 respectively. The main reason for the relatively large difference in number of observations is the swath width that is 247 km for PR and 878 km for TMI (see also Negri et al., 2002; Nesbitt et al., 2004). We note that the products represent snapshots of rainfall rates and have temporal frequency of 1 or 2 observations per day depending on the latitude.

PR (2A25) has horizontal resolution of 5 km × 5 km while TMI (2A12) has resolution of 5 km × 12 km. The products are processed by the TRMM science team using the algorithms described in Iguchi et al. (2000) and Meneghini et al. (2000). TRMM products can be downloaded free-of-charge following the link http://daac.gsfc.nasa.gov/precipitation.

In addition to satellite rainfall data, a Digital Elevation Model (DEM) of 90 m resolution from Shuttle Radar Topography Mission (SRTM-version 4) (http://srtm.csi.cgiar.org/) is used to extract a DEM of the study area. This DEM is used to delineate the basin boundaries and to extract the major river drainage network of the study area (see Fig. 1). In addition, the DEM is used to assess the effect of topographical characteristics such as elevation on the spatial distribution of rainfall in the UBN basin.

2.3. Ground observations

Rainfall estimates from satellites may have substantial errors (see Sapiano and Arkin, 2009; Haile et al., 2012a) and therefore estimates require validation using ground based observations. For this study we collected ground based rainfall data from the National Meteorological Agency of Ethiopia (NMA) (www.ethiomet.gov.et). In the study area continuous recording rain gauges are installed only in Mekane-Selam, Shawura and Fiche and time series of hourly rainfall data for the wet season period JJAS (2002–2005) were constructed. We used these 24 hourly time series to evaluate the accuracy of the diurnal cycle results from the satellite products. The latitudinal and longitudinal locations and elevation of the three stations are given in Table 1. The locations of the rain gauges are shown in Fig. 1. To broaden the assessment how well TRMM-based accumulated diurnal rainfall estimates match to ground observations we selected time series for 9 collector stations from National

Table 1
Latitude and longitude of the stations and corresponding elevations.

Station name	Latitude	Longitude	Elevation (m)	Type
Mekane-Selam	10°45′N	38°45′E	2600	Recording
Shawura	11°56′N	36°52′E	2232	Recording
Fiche	9°48′N	38°42′E	2750	Recording
Dangila	11°15′N	36°51′E	2127	Collector
Gondar	12°30′N	37°25′E	1985	Collector
Debre tabor	11°53′N	37°59′E	2535	Collector
Enjibara	10°00′N	36°54′E	2592	Collector
Adet	11°16′N	37°29′E	1950	Collector
Ageregenet	11°55′N	38°10′E	1985	Collector
Wanzaye	11°48′N	37°40′E	1984	Collector
Maksegnit	12°21′N	37°29′E	1970	Collector
Sekela	11°00′N	37°13′E	2715	Collector

Meteorological Agency (NMA) covering the period 2002–2008 and compared the TRMM estimates to the mean annual rainfall depth.

3. Methodology

The processing of TRMM Level-2 PR-2A25 and TMI-2A12 products involved extraction using the TRMM Orbit Viewer at (ftp://disc2.nascom.nasa.gov/software/trmm_software/Orbit_Viewer/) and conversion of the TRMM products in ASCII table format to Geographic Information System (GIS) maps using the Integrated Land and Water Information System (ILWIS) (http://52north.org/communities/ilwis/overview). The processing of the image samples in ILWIS involved geo-locating the images and inverse distance interpolation of the image sample points to yield raster maps. For both PR and TMI inverse distance weighting (power 2) is applied and samples are interpolated to maps with resolution of 5 km × 5 km. Such unified resolution allows comparison of results by map overlay. Next, images that are acquired at similar moments in local time are stratified by their Local Standard Time (LST) at 1-hourly time interval to assess the diurnal cycle. By use of ILWIS we analysed the TRMM sampling frequency, the frequency of rainfall occurrence and the mean rain rate.

3.1. Statistics of the diurnal cycle

In the procedure, summary statistics that include count, sum, mean, standard deviation and coefficient of variation are used for assessments. The number of TRMM observations is counted for each pixel for each LST to assess the frequency and uniformity of sampling. Uniformity of sampling across the study area is assessed by estimating the coefficient of variation (Cv) where lower Cv values indicate more uniform sampling.

$$Cv_i = \frac{\sigma_i}{\mu_i} \tag{1}$$

with mean (μ) and standard deviation (σ) estimated as follows:

$$\mu_i = \frac{\sum_{t=1}^{N} f_i^t}{N} \tag{2}$$

$$\sigma_i = \left(\frac{\sum_{t=1}^{N} (f_i^t - \bar{f}_i)^2}{N-1} \right)^{0.5} \tag{3}$$

where f refers to an observation, i refers to a pixel, t refers to Local Standard Time, N is total number of hours (24) in a day and $\bar{f}_i$ is the average of f for a respective pixel i.

For assessing the spatial distributions of the mean rain rate and the frequency of rainfall detection by the satellite, rainfall at pixel level is identified using a rainfall detection threshold of 1 mm h^{-1} (see Kummerow et al., 1998; Nesbitt and Zipser, 2004; Haile et al., 2010). In the following the frequency of rainfall detection by TRMM is referred to as rainfall occurrence (RO) in % at each LST and is defined as:

$$\mathrm{RO} = \frac{\sum_{1}^{\mathrm{TN}} N_t}{\mathrm{TN}} \times 100 \tag{4}$$

where N_t is 1 at selected Local Standard Time (LST) if the rain rate $\geq$1 mm h^{-1}; TN is total number of TRMM observations for a selected LST.

To eliminate the effect of non-rainy periods on the statistics, for each selected LST the conditional mean rain rate (RR) in mm h^{-1} that is conditioned on the detection threshold of 1 mm h^{-1} reads:

$$\mathrm{RR} = \frac{\sum_{1}^{\mathrm{TN}} \text{rain rate}}{N_t} \tag{5}$$

3.2. PR and TMI conditional mean rain rate comparison

When comparing PR and TMI conditional mean rain rates for the detection threshold 1 mm h^{-1}, PR observations are deducted from TMI observations for selected LST on pixel basis. The resulting difference maps are classified into 3 classes that are PR = TMI, PR > TMI and PR < TMI which indicate where the PR and TMI rain rates match or differ (i.e. higher or lower) over the UBN basin. The difference map serves to assess possible regional characteristics of the disagreement between PR and TMI rain rates. Further, percentage areas across the study area are calculated for selected LST to evaluate how well observations match. We note that for the mean rain rate comparisons, the assumption is that the difference in swath widths between PR (247 km) and TMI (878 km) has little effect on the conditional mean rain rate (see Ikai and Nakamura, 2003).

3.3. Comparison of PR and TMI estimates with ground observations

Comparing satellite based rainfall estimates to ground based estimates by gauging stations is not straightforward by issues that relate to the scale of observation. Satellite based microwave sensors such as PR and TMI rely on instantaneous measurements of microwave radiances from the cloud system to make an estimate of rain rates for spatial domains defined by the image resolution (i.e. the foot print area or pixel size). Ground based rain gauges provide accumulated rainfall over the observation time period but only at a point scale (i.e. the size of the gauge funnel). To allow comparisons between satellite products and ground based observations, in this study we assume that the variability of rainfall within the (pixel) foot print area (i.e. 5 km × 5 km) of the interpolated satellite image samples may be ignored and thus rain gauge data may be compared to the pixel based satellite observations. Obviously ignoring rainfall variability at spatial scales of 5 km × 5 km may affect results of comparison particularly when variability of real world characteristics such as elevation and slope gradient is high or simply when the slope aspect from a hill slope changes from windward to leeward (see Camberlin, 1997). We note that in Haile et al. (2009, 2011) significant variability in rain event properties in space and time dimensions is indicated by use of a rain gauge network of 8 continuous recording stations that cover the Upper Gilgel Abay catchment (1656 km^2) at the source area of the UBN.

Comparison of TRMM observations to ground-based observations is performed for diurnal cycle characteristics of rainfall occurrence and conditional mean rain rate. For this purpose PR and TMI pixels that overlay the locations of the rain gauges are selected. Since the threshold applied for the TRMM satellite data is 1 mm h^{-1}, the same threshold is applied for the ground based observations. We note that rain gauge data is available only for the period 2002–2005 and assume that seasonal averages of the rain

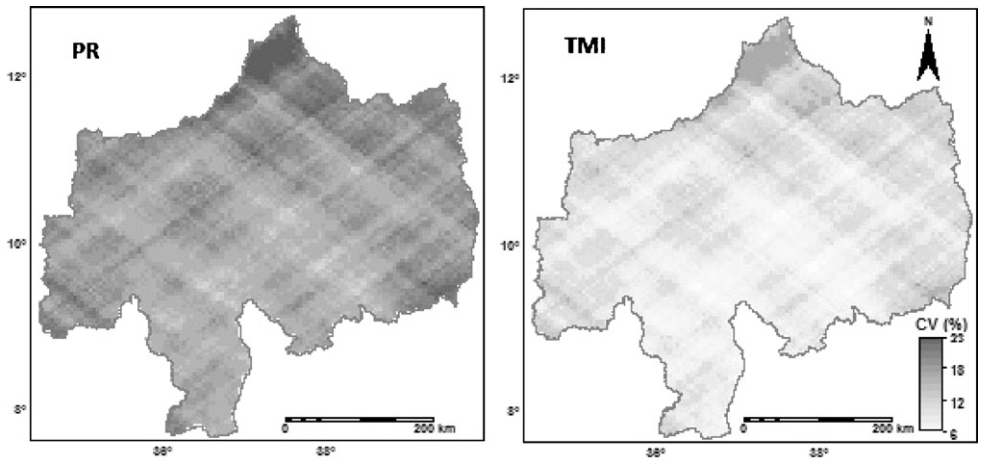

Fig. 2. Coefficient of variation of the number of observations of Precipitation Radar (PR) and TRMM Microwave Imager (TMI) (JJAS, 2002–2008).

gauge data from 2002 to 2005 are representative for the period of the satellite observations (2002–2008). The limited sample size of ground observations is typical for less developed countries like Ethiopia and stresses the importance to further analyse the effect of non-representative of rain gauges when evaluating performance of satellite products (see Haile et al., 2012a).

3.4. Spatial variability of rainfall

Rainfall distributions in mountainous areas and plain areas differ by effects of topography and local climatic settings (e.g. Arora et al., 2006). To assess how diurnal cycle properties of rainfall occurrence and mean rain rate across the basin area are affected by topography two transects are taken. Transect WE serves to assess the diurnal cycle variability in west to east (WE) direction that possibly is affected by the low land areas in the south-west of the basin, the Blue Nile River gorge, Choke-mountain, and the ridges in the northeast of the basin. Transect NS points from north to south (NS) and crosses Lake Tana, Choke-mountain and the Blue Nile gorge. Transects are selected in such a way that they cross the gorge at different locations so to assess the diurnal cycle of rainfall over various topographic features. Results are shown graphically for selected LST.

3.5. Estimation of daily rainfall

From the mean hourly rain rate and rainfall occurrence maps the accumulated rainfall depth (RD) for the rainy season (JJAS) is estimated. We note that the sample size of rainfall occurrence for individual pixels changes across the study area since observations for each pixel are not available for each LST for each day. As described in Section 2, for the period 2002–2008 the number of observations for each pixel and for each LST was in the range 8–20 for PR and in the range 37–50 for TMI with means of 13 and 43 respectively. Daily rainfall is estimated simply by summing the rainfall depth maps for each LST that is the product RR × RO. The rainfall depth for the rainy season is estimated as follows:

$$\mathrm{RD} = \sum_{\mathrm{LST}=1}^{24} (\mathrm{RR} \times \mathrm{RO}) \times \mathrm{TD} \tag{8}$$

where LST is Local Standard Time, 24 is the number of hours in a day, TD is the total number of days during the rainy season (120 days). We broaden the rainfall depth assessment by comparing the 24-h accumulated diurnal cycle estimates of TRMM to time series from some additional 9 collector stations.

4. Results and discussion

4.1. Uniformity of sampling

Uniformity of sampling in terms of *Cv* (Eq. (1)) for PR and TMI for 1-hourly period is indicated in Fig. 2. For PR *Cv* ranged from 12 to 23% and compare to results by Negri et al. (2002) who had *Cv* values in the range 8–22% for a 4-hourly period. Given that our sampling is at hourly time step we consider *Cv* values for our image data as relativley low and thus suggests relatively homogeneus sampling across the basin area. We note that our sample was based on 7 years of data compared to three years of data in Negri et al. (2002) that, presumably, positively affected our smapling result. *Cv* values of TMI have value range of 5–9% (Fig. 2) and are much lower compared to those of PR. The more uniform sampling of TMI presumably is a result of the much wider swath width of TMI. Based on these results, we consider estimates of rainfall by TMI to be more representative than estimates by PR.

4.2. Rainfall diurnal cycle

4.2.1. Rainfall occurrence

Fig. 3 shows the PR based diurnal distribution of hourly rainfall occurrence over the UBN basin for JJAS. Results indicate clear time–space variability with maximum rainfall occurrence between 36% and 50% for respective Local Standard Time (LST). Over the 24-hourly period, rainfall occurrence shows a pattern with relatively high values over large spatial domains during late evening and early morning hours (20:00–05:00 LST). Lowest values are observed between 06:00 and 12:00 LST except for some isolated locations with high rainfall occurrence. The diurnal distribution shows rainfall occurrence (up to 50%) in the mid afternoon to early evening hours (15:00–20:00 LST) over large parts of the basin but areas of the Blue Nile River gorge (shown by the thin dark grey line) only have relatively low occurrence. Areas along the Blue Nile River gorge show a pattern that is different from surrounding areas with rain occurrence that is highest during the evening between 20:00 and 23:00 LST. Over Lake Tana and around Fincha reservoir (see Fig. 1), highest rainfall occurrence is observed during late evening to mid-night hours between 22:00 and 00:00 LST.

Similar results over the southern shore of Lake Tana were found by Haile et al. (2009) using 3 month (June–August 2007) of rainfall data from a network of 8 recording rain gauges and a remote sensing based convective index from infrared (IR) images of the Meteosat Second Generation (MSG-2) satellite (see http://www.eumetsat.int/Home/Main/Satellites). Moreover, they

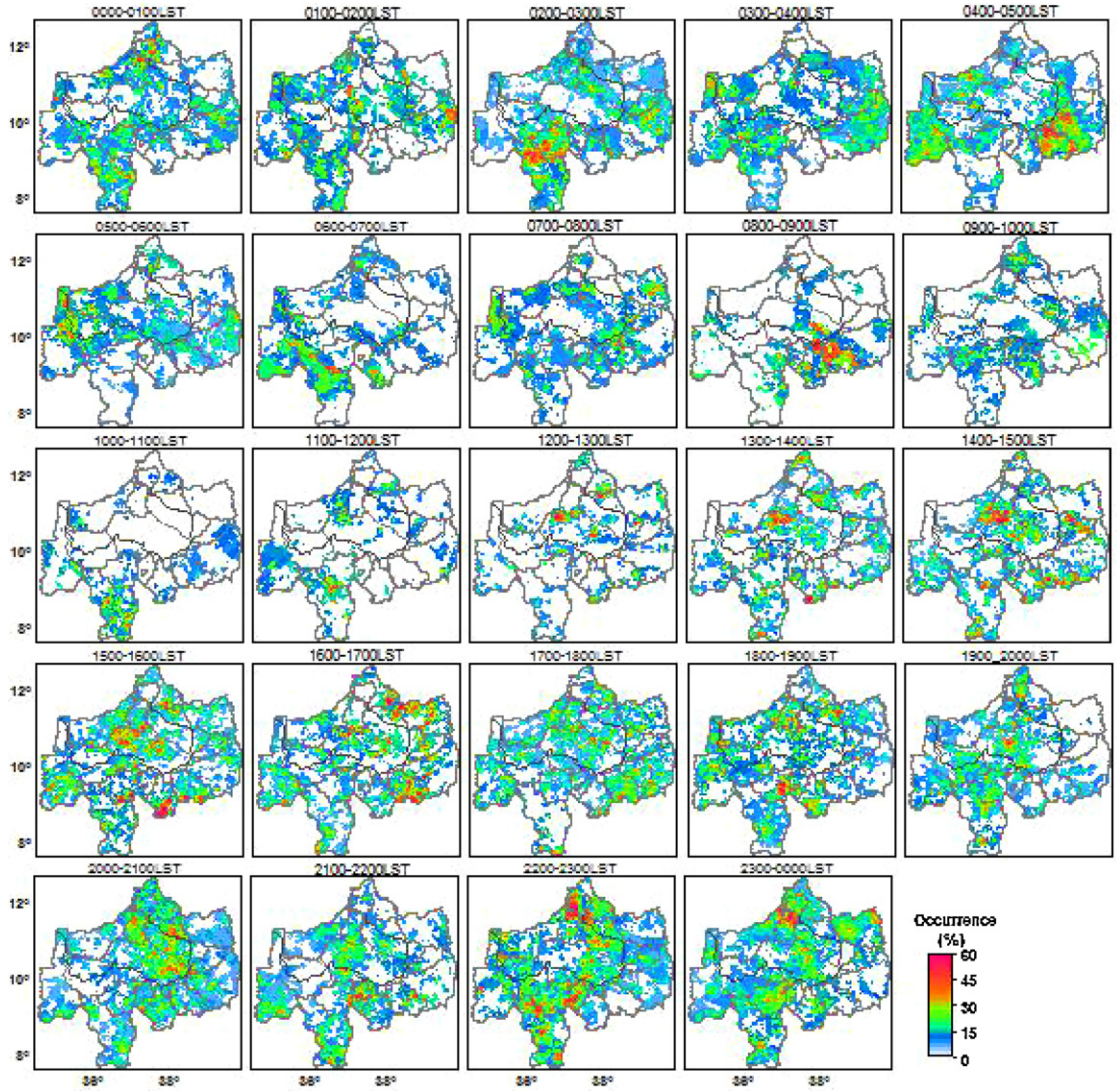

Fig. 3. Diurnal cycle of rainfall occurrence using Precipitation Radar (PR) data (JJAS, 2002–2008).

also found mid to late afternoon highest rainfall occurrence and convective activity around the ridges of Gilgel Abay catchment that is located in the Lake Tana basin area. This is in agreement with the results of this study in highest rainfall occurrence around the ridges of Gilgel Abay is observed in the late afternoon (16:00–18:00 LST) as well.

The diurnal cycle distribution of rainfall occurrence for TRMM Microwave Imager (TMI) is shown in Fig. 4 and resembles the cycle by PR with relatively high rainfall occurrences at certain LST and certain spatial domains. TMI differs from PR in a manner that TMI indicates occurrence of rainfall over larger spatial domains where occurrence more gradually changes. Further, the comparison shows that many pixels with occurrence zero for PR have values higher than zero for TMI. Values of highest occurrence for TMI suggest a larger range (28%) than for PR (14%) while TMI has higher maximum (60%) compared to PR (50%). Similar to PR, rainfall occurrence is low between 06:00 and 13:00 LST over most parts of the basin. In the south-western and western part of the basin high rainfall occurrence is observed during night time and early morning hours (01:00–06:00 LST). Over most parts of the basin the rainfall occurrence is highest during mid to late afternoon (15:00–18:00 LST). In the areas along the Blue Nile gorge, Lake Tana and Fincha reservoir, highest rainfall occurrence is observed from 22:00 to 00:00 LST.

4.2.2. Conditional mean rain rate

The PR result of the diurnal distribution of conditional mean rain rate is shown in Fig. 5. Over most areas of the basin, the rain rates are lowest between 06:00 and 15:00 LST with exceptions for Didessa, Dabus, Jemma and Muger sub-basins that are located in the south-west part of the study area. Results in Fig. 5 indicate that in these sub-basins the conditional mean rain rate is highest between midnight and early morning (00:00–06:00 LST). Large parts of the study area show a high conditional mean rain rate between 15:00 and 18:00 LST. Over Lake Tana and along many stretches of the UBN River, high mean rain rates are observed during 18:00–00:00 LST and 20:00–23:00 LST, respectively. Similar results with high rain rates observed during midnight are found in Barros et al. (2004) in a study over long (>100 km) wide valleys (>10 km) in the Aravalli mountain range (Himalayas). It was further described that the midnight maximum rain rate in the valley could be related to the complex topography.

The TMI result of the diurnal distribution of conditional mean rain rate is shown in Fig. 6. Conditional mean rain rates in general are highest for late afternoon and evening hours (15:00–00:00 LST) and lowest for morning and early afternoon hours (06:00–14:00 LST). Highest rain rates (20 mm/h) are most frequently observed in the west and south-western parts of the basin. The distribution

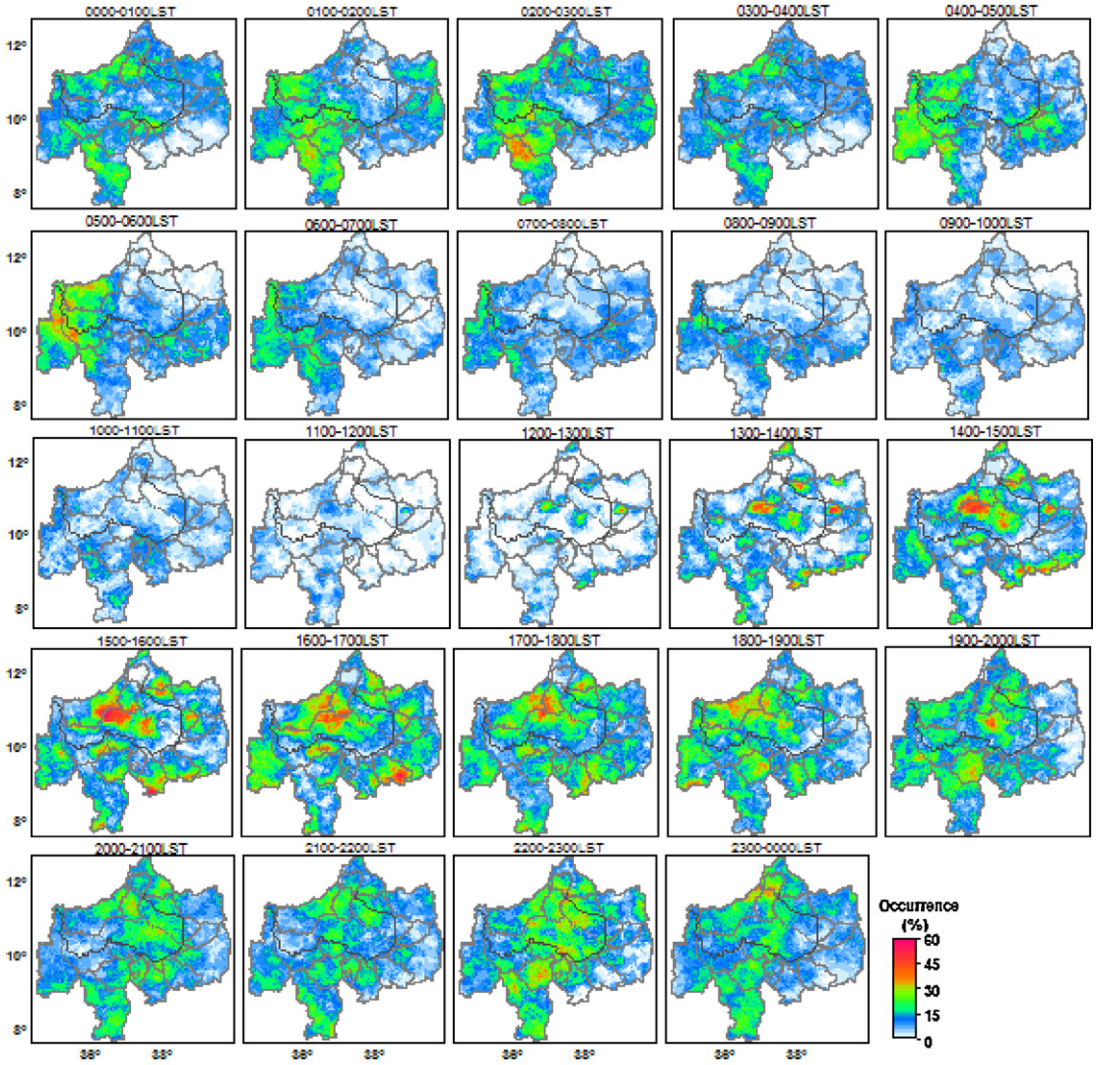

Fig. 4. Diurnal cycle of rainfall occurrence using TRMM Microwave Imager (TMI) data (JJAS, 2002–2008).

of these rain rates is uneven across the UBN basin suggesting the convective nature of rainfall in the study area. Exceptions to this pattern are observed at morning hours (09:00–10:00 LST) in the northern part of the basin. We note, however, that rainfall occurrence is low for this LST and location and thus the high rain rates are not necessarily representative. Lowest values of mean conditional rain rate for each LST are mostly in the central part of the basin area and along the wide and deeply incised gorge of the UBN River.

4.3. Comparing mean rain rate for PR and TMI

To compare the conditional mean rain rate estimates from PR and TMI, the difference between the rain rate estimates is calculated and the resulting map is classified into three classes as: PR > TMI, PR = TMI and PR < TMI (see Fig. 7). The comparison is at 05:00–06:00, 11:00–12:00, 17:00–18:00 and 23:00–00:00 LST to represent morning, midday, afternoon, and midnight times, respectively. Table 2 shows the percentage of the areas of each class for the selected time periods.

Table 2 and Fig. 7 indicate that the PR and TMI observations have similar conditional mean rain rate over most parts of the basin (62%) during midday (11:00–12:00 LST). For the other LSTs, the TMI estimates are higher than PR estimates by 42–51% over most of the basin. We note that during midday large areas are indicated for which no rain is observed by both PR and TMI and thus contribute to the high % match (62%) between PR and TMI rain rates. In the late afternoon (17:00–18:00 LST), late evening (23:00–00:00 LST) and morning (05:00–06:00 LST), TMI has higher values than PR over large parts of the study area as a result of the relative high rain rate values of TMI and the relatively large area for which rain is detected in TMI. The latter particularly applies to the southern part of the basin area. We note that Kummerow et al. (2000), Negri et al. (2002) and Nesbitt et al. (2004) also reported higher rain rate values for TMI as compared to PR over land surfaces. Nesbitt et al. (2004) attributed the disagreement to the biases associated with the empirically derived 85 GHz ice-scattering rain rate relationship of TMI.

Table 2
The percentage of areas under each class (PR > TMI, PR = TMI and PR < TMI) for the selected Local Standard Time (JJAS, 2002–2008).

	05:00–06:00	11:00–12:00	17:00–18:00	23:00–00:00
PR > TMI	23	14	27	25
PR = TMI	35	62	22	26
PR < TMI	42	24	51	48

PR, Precipitation Radar; TMI, TRMM Microwave Imager.

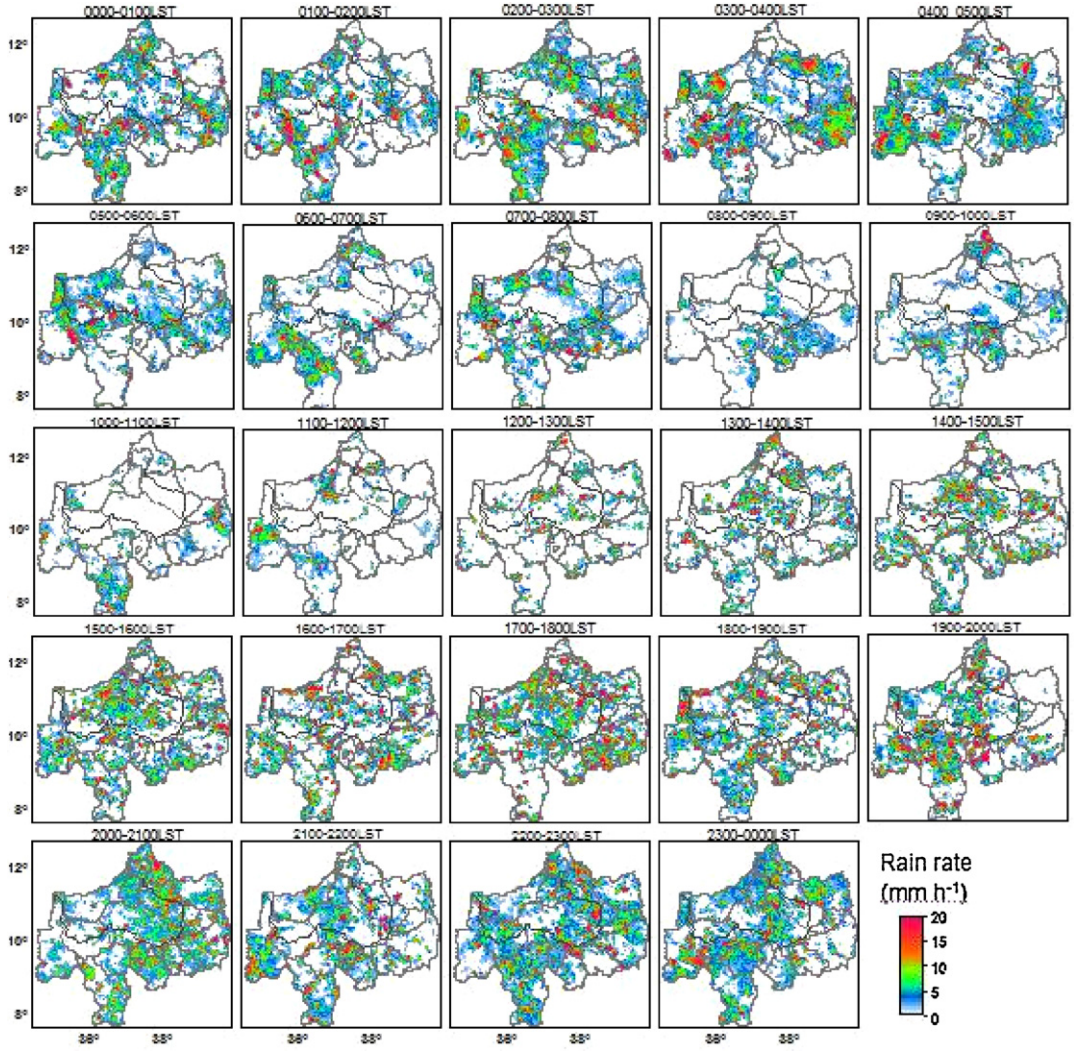

Fig. 5. Diurnal cycle of conditional mean rain rate using Precipitation Radar data (JJAS, 2002–2008).

4.4. Diurnal variability with terrain elevation

In Ikai and Nakamura (2003) it is reported that PR-rain rates are higher than TMI-rain rates in mountainous regions such as the Rocky-mountains, the Andes, and the Himalayas. Assessing how relief affects rainfall, Kuraji et al. (2001) indicated that rainfall occurrence from the two TRMM instruments can show pronounced differences while differences in rain rates only are relatively small. Both statements, however, suggest that relief affects rainfall properties. Since the UBN basin is characterised by high variation of terrain elevation, a wide and deeply incised river gorge and the presence of large mountain ranges in the centre of the basin and at the eastern and the northern catchment divides we assessed effects of relief as well. Along two transects from the north to south-east (NS) and from west to east (WE) directions (see Fig. 1) we assessed the time–space patterns of the diurnal cycle of rainfall occurrence and conditional mean rain rate for both PR and TMI. For graphical presentation of results we refer to Figs. 8–10.

For the WE transect results indicate that rainfall occurrence ranges from 0 to 40% with maximum occurrence observed on the windward sides of mountainous areas for both PR and TMI during afternoon and evening hours (12:00–00:00 LST) while occurrence is low on the leeward side (see Fig. 8). This pattern is less clearly observed in the NS transect with highest values south of the UBN river gorge for TMI during afternoon hours (16:00–18:00 LST) and highest values for PR during night hours (03:00–06:00 LST) towards the Upper Blue Nile (UBN) catchment divide at the south end of the transect (see Fig. 8).

Results suggest the existence of orographic influences by the high mountain ranges and the deep river gorge. As described in Section 2, the general air circulation pattern in the Blue Nile basin is characterised by south-westerly flow and hence rainfall in the mountainous areas with west, south-west and south facing mountain slopes (windward slopes) and north, north-east and east facing mountain slopes (leeward slopes) can be affected. We note that particular for PR in gorges A and B relatively low occurrence is observed while the west facing slopes have higher occurrence. Along transect NS, which crosses Lake Tana, Choke-mountain and the Blue Nile gorge, the rainfall occurrence is maximum around midnight over Lake Tana. There is some variation in the pattern of the diurnal cycle around and over Lake Tana suggesting that the presence of the lake has an effect on rainfall distribution. This aspect is further discussed in Haile et al. (2009) where a satellite based convective index is used to indicate the effect of Lake Tana on diurnal rainfall properties.

On the north-west side of Choke-mountain (see Fig. 8) rainfall occurrence is higher than on the south-east side and suggests that relief affects rainfall occurrence. South-east of the Blue Nile gorge at D (Fig. 8) early morning maximum rainfall occurrence is observed for both the PR and TMI observations. Rain occurrence is

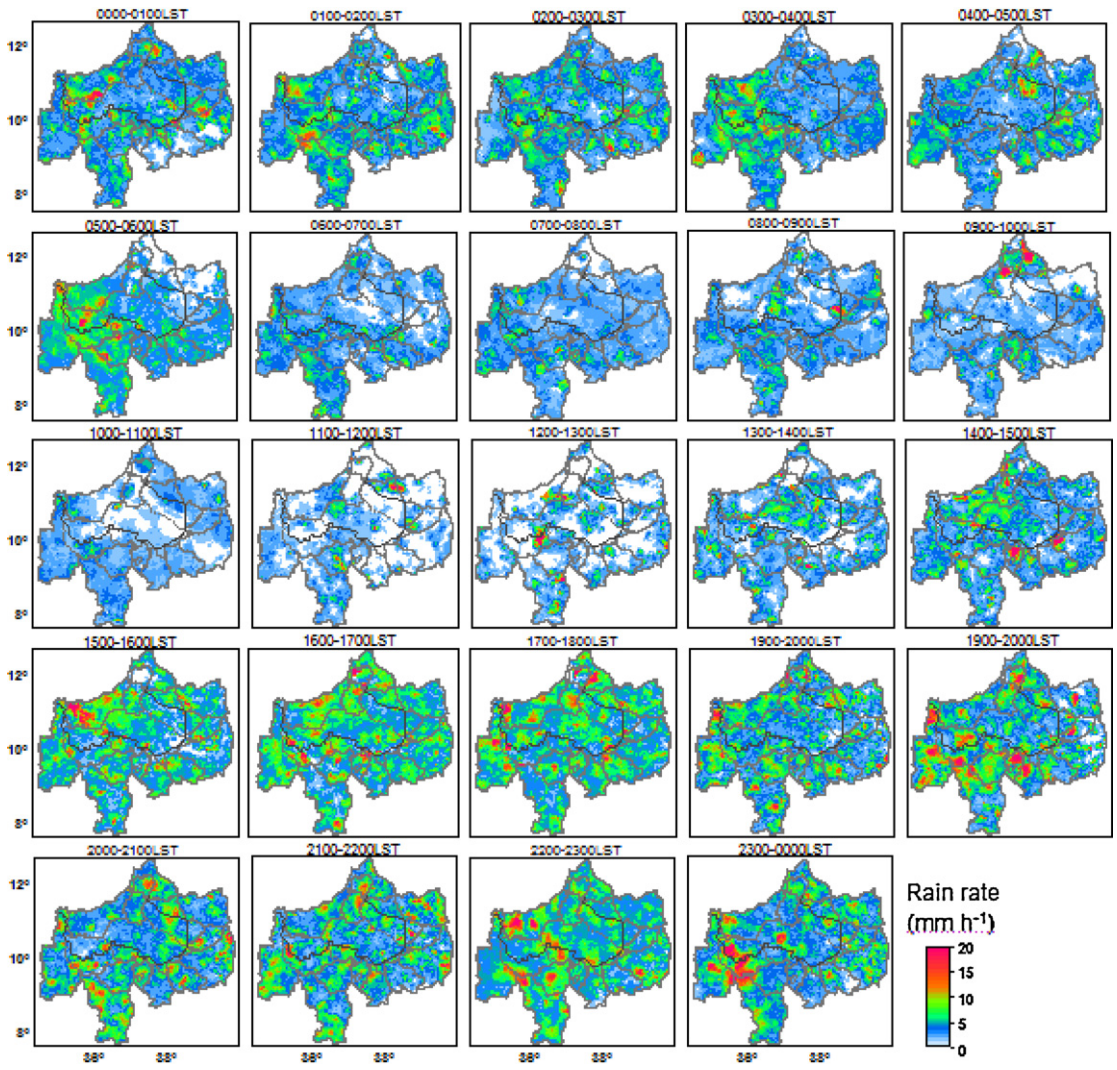

Fig. 6. Diurnal cycle of conditional mean rain rate using TRMM Microwave Imager (TMI) data (JJAS, 2002–2008).

highest for midnight to early morning hours where PR occurrence is higher than TMI. However, further to the south-east an afternoon maximum is observed from both PR and TMI observations.

To further assess the effect of relief we plotted PR and TMI rainfall occurrence along transect WE with the terrain elevation added. The LST is selected at 6-h interval and as such the assessment is done for morning, midday, afternoon, and midnight times.

Results for both PR and TMI indicate a clear increasing trend of rainfall occurrence with terrain elevation particularly for 17:00–18:00 and 23:00–00:00 LST, however, this pattern is not very pronounced for night and morning hours. Highest occurrence is not at highest mountain elevations but on elevated areas on the windward sides while occurrence is low for the areas on the leeward side. A similar pattern is described in Haile et al. (2009) who evaluated time–space variability of rainfall in the mountainous Gilgel Abay catchment that is the source area of the Blue Nile River. Results in Fig. 9 further indicate that for most selected LSTs the estimated rainfall occurrence for TMI is higher than for PR. A direct relation between rainfall occurrence and terrain elevation is also evident from transect in north to south-east (NS) direction for 17:00–18:00 LST although for other LSTs, such relation could not be clearly identified. In most of the observations the TMI estimates are higher than PR estimates.

Results of the conditional mean rainfall rate along both transects are shown in Fig. 10. For transect in west to east (WE) direction it is shown that for both Precipitation Radar (PR) and TRMM Microwave Imager (TMI) the highest afternoon mean rain rate is observed in the lowland areas that are situated north-east of gorge A. The mean rain rate reaches highest value during the night time in gorge A but for gorges B and C a pronounced highest value is not observed and indicates variability in the mean rain rate along the UBN river gorge. In the south-western part of Choke-mountain an afternoon highest mean rain rate is observed for TMI while PR observations reveal late afternoon to midnight highest values. The mean rain rate at the opposite side of Choke-mountain (north-eastern part) is lower than the areas in the south-west of the mountain which can be attributed to the rain shadow effect. Along both transects over most of the LSTs, the mean rain rate estimated from TMI is higher than PR with an exception of some local points.

Along transect NS, the pattern of conditional mean rain rate (see Fig. 10) shows night time highest values over Lake Tana for PR and TMI observations. Moreover, the mean rain rate in the southern part of the lake is higher than the northern part. This is in agreement with Haile et al. (2009) who found highest cloud convection during night time over the southern shore of the lake using data from an experimental network of 8 recording stations. Over the Blue Nile gorge at point D, the highest mean rain rate is observed in the early morning for the PR observations while highest rain rates are observed during night hours for TMI. We

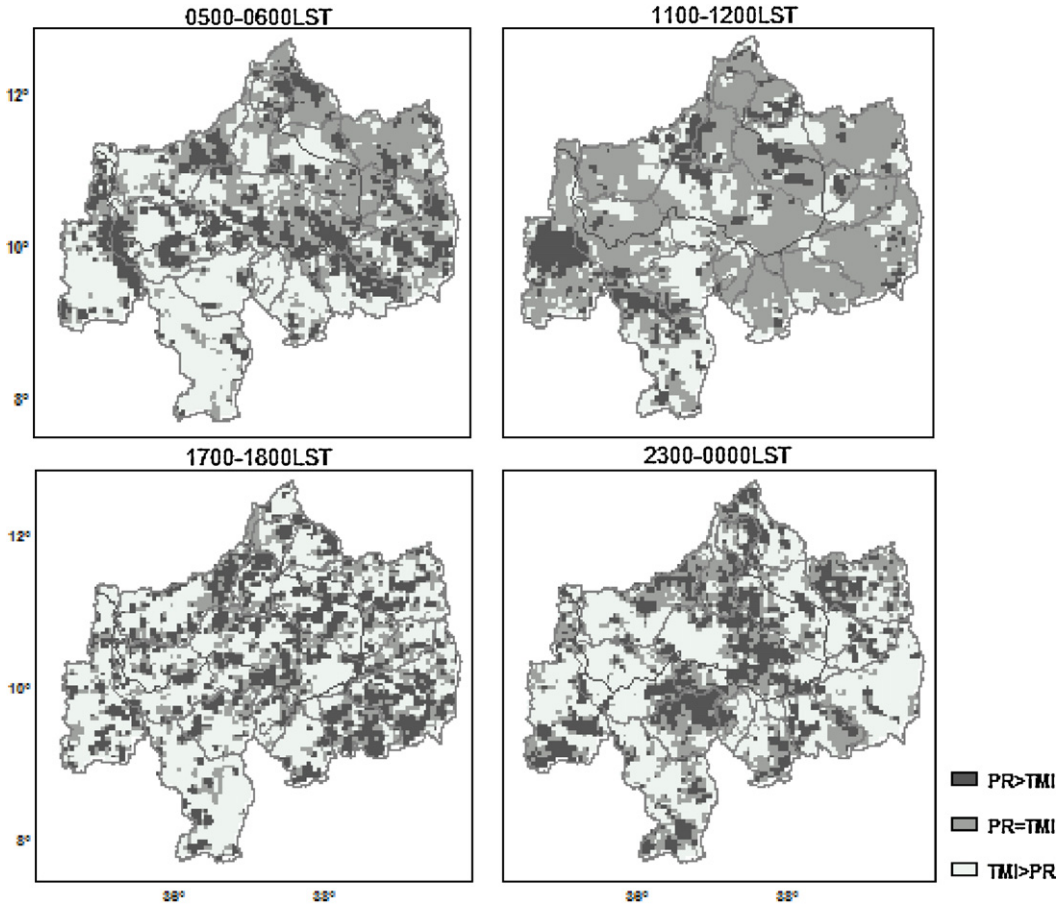

Fig. 7. Comparing Precipitation Radar (PR) and TRMM Microwave Imager (TMI) observations of mean rain rate for selected Local Standard Time (LST) (JJAS, 2002–2008).

note that TMI indicates that a larger area north of Choke-mountain receives rainfall when compared to PR although the highest rain rates for TMI in general are lower as compared to PR. Along transect NS it is shown that the mean rain rate distribution is affected by relief and that highest rates across the gorge differ for respected LSTs.

4.5. Rainfall depth estimation from PR and TMI observations

Results of estimation of the wet seasonal rainfall depth (Eq. (8)) from PR and TMI observations are shown in Fig. 11. Results of PR indicate higher spatial variability as compared to TMI where gradual changes of rainfall depth are shown over larger spatial domains.

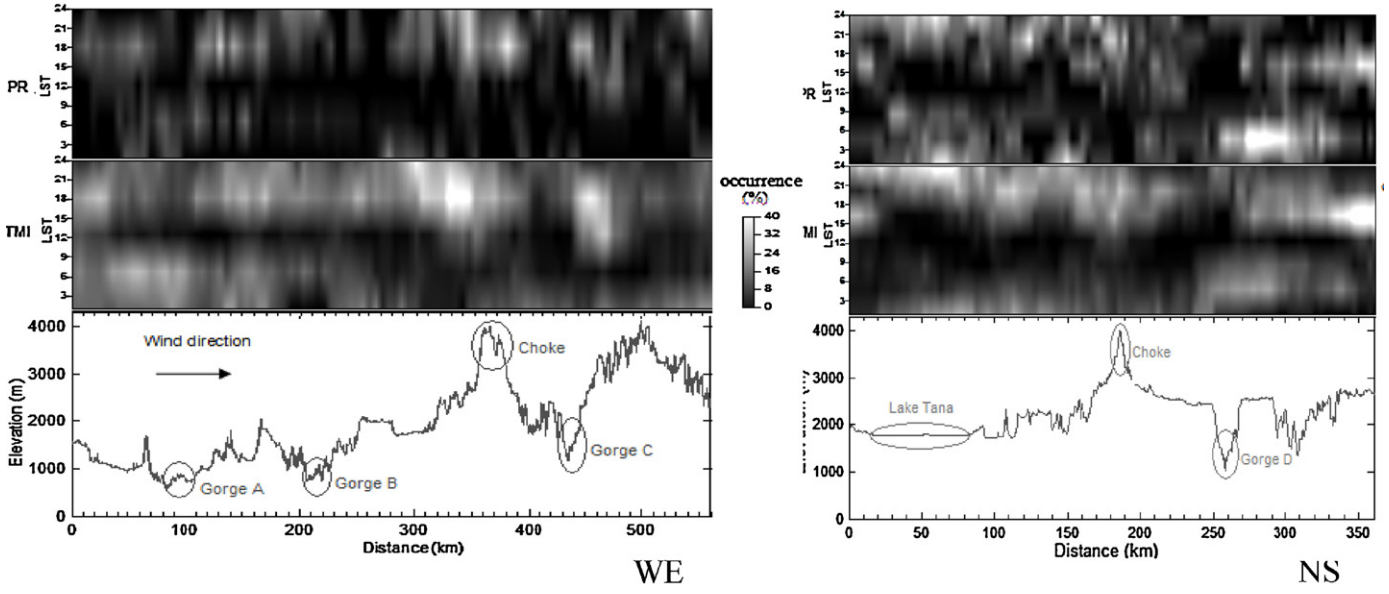

Fig. 8. Diurnal cycle of rainfall occurrence along transect from west to east (WE) and from north to south-east (NS) (JJAS, 2002–2008).

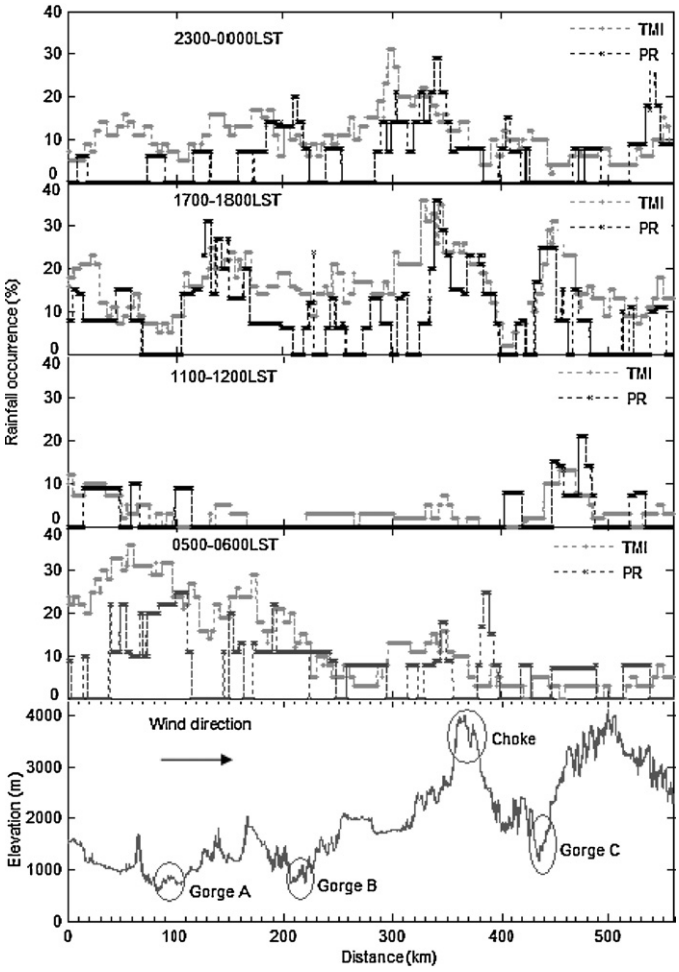

Fig. 9. Rainfall occurrence of Precipitation Radar (PR) and TRMM Microwave Imager (TMI) along transect from west to east (WE) for selected Local Standard Time (JJAS, 2002–2008).

Further, PR indicates variation with high and low values across the entire basin area whereas TMI indicates that in the western part of the catchment in general the highest rainfall depths are observed while the eastern part in general has lowest rainfall depths. For PR, highest rainfall is indicated north-east of Choke-mountain and in elevated areas east of the river gorge in the south-west. For TMI high rainfall is observed at similar locations as for PR by relatively high rain rates and rain occurrence. For TMI high rainfall is also observed in particular areas in the east of the basin. Both PR and TMI indicate low rainfall depth along the areas of the river main stream in the central part of the basin.

Conway (2000) reported that the areas in the south-west of the basin receive higher amounts of annual rainfall (>1600 mm) compared to the north and northeast parts (around 1000 mm) and 70% of the annual rainfall occurs during the wet season that covers the months June, July, August and September (JJAS). According to UNESCO (2004), Kim and Kaluarachchi (2008) and Abtew et al. (2008), the annual rainfall over the basin ranges from 1200 mm to 1600 mm. In this study, maximum rainfall depth as observed by PR and TMI also is in the order of 1600 mm but minimum values of PR and TMI are much lower with an extreme low value of 100 mm. We note that the low values could be influenced by the limited number of observations (see Section 2) for certain pixels (see also Fig. 2). Therefore, for areas with high variability the sample size not necessarily is large enough to produce representative rainfall estimates for all pixels and possibly the extreme low rainfall depth may not be representative to allow for generalisation. On the other hand, the rain gauge network of National Meteorological Agency (NMA) only has very poor density and therefore for most locations in the basin ground data is missing. We note that driest locations are indicated in PR in the north-east and the west that are characterised by low rainfall occurrence but also low rainfall rate.

4.6. Evaluation of PR and TMI estimates using ground observations

For evaluation of results of PR and TMI we compared the satellite observations to ground observations. The comparison is for three recording stations that are located in different parts in the basin (see Fig. 11). It is noted that these stations are the only recording stations available by NMA in Ethiopia. The comparison is for pixel values

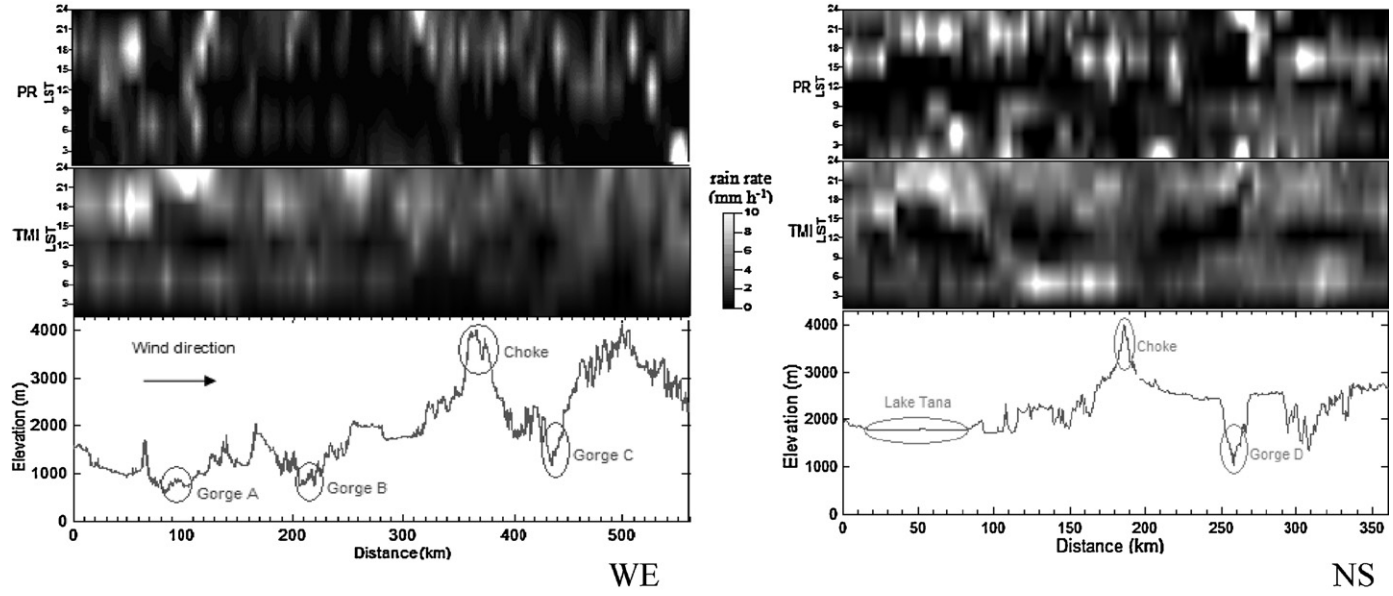

Fig. 10. Diurnal cycle of conditional mean rain rate along transects from west to east (WE) and from north to south-east (NS) (JJAS, 2002–2008).

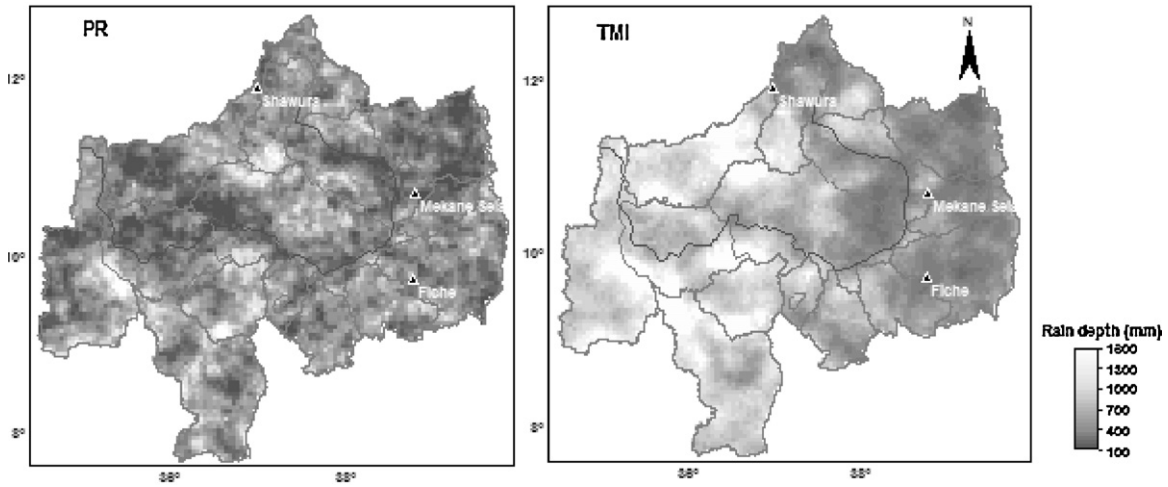

Fig. 11. Precipitation Radar (PR) and TRMM Microwave Imager (TMI) estimated wet seasonal rainfall depth (JJAS, 1998–2008).

of PR and TMI that overlay the locations of the gauges at Fiche, Mekane-Selam and Shawura stations. Bar graphs in Fig. 12 indicate that the gauge based diurnal cycle distributions of the three stations show different patterns for the rain occurrence with highest occurrence observed in the early morning, afternoon and midnight hours, for Fiche, Mekane-Selam and Shawura stations respectively. In general, the pattern of the diurnal cycle of rainfall occurrence from PR and TMI estimations reasonably match with the ground observations although some very large differences are shown when rainfall occurrence is highest for Mekane-Selam in afternoon Local Standard Times (LST) and for Shawura during late evening and early morning LSTs. The bar charts further indicate that rainfall

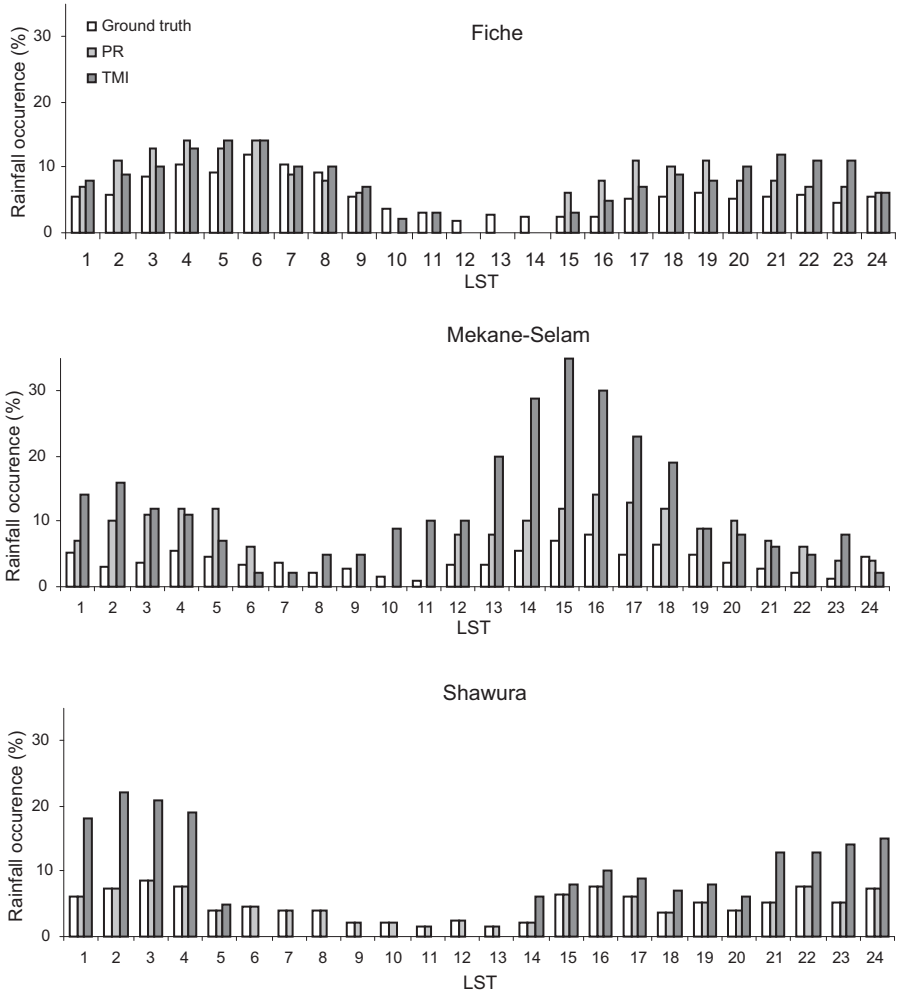

Fig. 12. Diurnal cycle of rainfall occurrence from Precipitation Radar (PR), TRMM Microwave Imager (TMI) and ground observations (JJAS, 2002–2008).

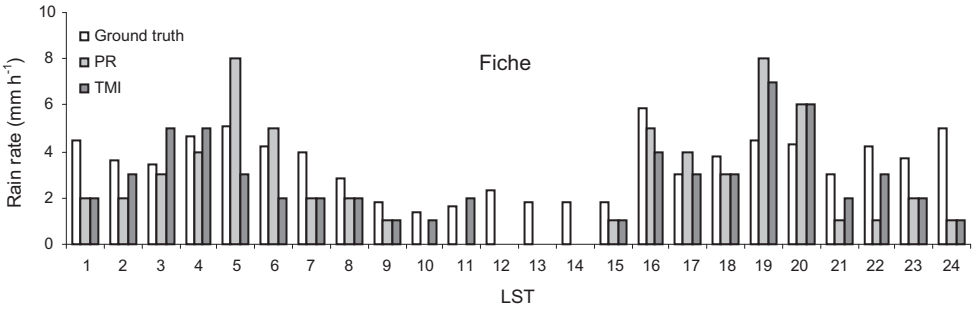

Fig. 13. Diurnal cycle of conditional mean rain rate from Precipitation Radar (PR), TRMM Microwave Imager (TMI) and ground observations for Fiche station (JJAS, 2002–2008).

occurrence from TMI in general is higher than PR but also that for most of the LSTs the ground observations have lowest occurrence. A possible reason for this could be that satellite pixels cover a relatively large spatial domain by the foot print area and thus rainfall may be detected while not observed by the rain gauge. For Shawura station occurrence for PR and the rain gauge is comparable. For Mekane-Selam station TMI indicates much higher occurrence than the rain gauge.

Fig. 13 shows the diurnal cycle of the PR and TMI conditional mean rain rate estimates with ground observations from Fiche station. This station is chosen as its rainfall observations show relatively better correlation with the satellite rainfall estimates compared to the other two stations. The station receives high rain rates in the morning and late-afternoon to evening LSTs. Unlike the rainfall occurrence, the patterns of the diurnal cycle of conditional mean rain rate observed from the PR and TMI do not show a reasonable match with the ground truth over the three station sites (not shown for Mekane-Selam and Shawura). The gauge rain rates are mostly higher than for PR and TMI whereas the difference between the PR and TMI rain rates is not very consistent. The fact that observations of PR and TMI are at pixel scale while gauges observe rainfall at point scale may have affected the comparison results. For instance, in Haile et al. (2012a) it is shown that the gauge representative error can become relatively large when comparing satellite–gauge rainfall rates at hourly time scale. In this study we ignored this aspect by lack of sufficient gauge data at high temporal resolution.

In Table 3 a comparison is made between the means of JJAS rainfall depth for the 3 recording stations (2002–2005) and the TRMM based counterparts (2002–2008) and between the 9 collector stations (2002–2008) and TRMM based counterparts (2002–2008). We note that the sample size for the comparison between the 3 recording stations and TRMM is dissimilar although series overlap for a period of 4 year. For the recording stations the table shows that TMI has highest rainfall depth for Mekane-Selam and Shawura stations but that ground observations at Fiche are highest. Largest difference between PR and ground observations is shown for Mekane-Selam while largest difference between TMI and ground truth is shown for Shawura. Results in Figs. 12 and 13 and Table 4 suggest very different performance of PR and TMI. For the collector stations, PR generally shows lowest JJAS when compared to gauge observations. TMI often shows highest estimate but in some cases underestimates the gauge observation. This matches to previous observations on diurnal cycle assessments of PR and TMI and further indicates the complexity to estimate spatial distributions of rainfall over large scale variable terrain.

For further assessment on the diurnal cycle we performed a correlation analysis (Table 4). The correlation analysis between the rainfall occurrence from PR and TMI estimates and the ground truth shows that both PR and TMI estimates compare reasonably to ground observations in Fiche with $r = 0.72$ and 0.78 respectively. The diurnal cycle estimates from PR are slightly better correlated for Mekane-Selam ($r = 0.75$) and Shawura ($r = 0.73$) than for TMI. Overall, the analysis shows that there is clear relation between the satellite-estimated diurnal cycle of rainfall occurrence and the ground observations for the three stations at 95% significance level. Results on mean rain rates indicate that there is no significant correlation between the satellite estimated and the ground observations particularly at Mekane-Selam and Shawura stations. However, correlation values suggest that the PR estimates are more correlated to the ground observations than the TMI estimates in all three stations. The correlation matrix indicates that at the station sites there is a significant correlation between the PR and TMI mean rain rate estimates at 95% significance level.

Table 3
Seasonal rainfall depth at the three station sites for June, July, August, September (JJAS) (highest values are in dark grey and lowest values are in light grey).

Station	Rainfall depth (mm)			
	Ground truth	PR	TMI	Type
Fiche	569	540	546	Recording
Mekane-Selam	428	586	728	Recording
Shawura	458	449	928	Recording
Dangila	1285	1056	1467	Collector
Gondar	935	768	709	Collector
Debre tabor	1156	1104	1364	Collector
Enjibara	1797	1344	1703	Collector
Adet	945	792	845	Collector
Ageregenet	1193	840	965	Collector
Wanzaye	1120	960	1007	Collector
Maksegnit	928	744	762	Collector
Sekela	1458	1248	1673	Collector

PR, Precipitation Radar; TMI, TRMM Microwave Imager.

Table 4
Correlation matrix for the three station sites.

	Rainfall occurrence			Rain rate		
	GT	PR	TMI	GT	PR	TMI
Fiche						
GT	1			1		
PR	0.72*	1		0.53*	1	
TMI	0.78*	0.81*	1	0.44	0.73*	1
Mekane-Selam						
GT	1			1		
PR	0.75*	1		0.47	1	
TMI	0.66*	0.63*	1	0.22	0.64*	1
Shawura						
GT	1			1		
PR	0.73*	1		0.3	1	
TMI	0.61*	0.81*	1	0.21	0.66*	1

GT, ground truth; PR, Precipitation Radar; TMI, TRMM Microwave Imager.
* Correlation at 95% significance level.

5. Conclusion

Wet season (June–September) rain rate estimates retrieved from PR and TMI sensors on board the TRMM satellite are used to assess various aspects of rainfall variability in the UBN basin for the period 2002–2008. Time–space variability is assessed by constructing diurnal cycle estimates for rainfall occurrence and mean rain rate. Homogeneity of satellite image sampling is assessed by the coefficient of variation. Difference between the PR and TMI estimates is evaluated and effects of large scale relief on rainfall variability are assessed by constructing transects in north to south-east (NS) and west to east (WE) directions that cross the basin area.

Results of this study indicate that due to its large swath width TMI provides a larger number of observations and more uniform sampling than PR for the UBN basin. On 1-hourly period, 8–20 and 37–50 observations with coefficient of variation of 12–23% and 5–13% are obtained from PR and TMI, respectively.

The diurnal cycle estimates of both rain occurrence and mean rain rate show large variation over the basin area. Over most areas (62% of the basin area) the PR and TMI rain rate estimates are similar during midday (11:00–12:00 LST) and are partly caused by the fact that during midday most of the areas do not receive rainfall. For most other LSTs and over most of the basin area the TMI rain rate estimates are higher than PR counterparts. TMI also shows higher rainfall occurrence over large parts of the basin for nearly all LSTs. Value ranges of both rainfall occurrence (%) and mean rain rates ($mm\,h^{-1}$) are larger for TMI (0–60% and 0–20 $mm\,h^{-1}$) than for PR (0–50% and 0–16 $mm\,h^{-1}$) and suggest larger variability for TMI.

Results of this study show that variability of rainfall is affected by large scale relief. By use of the NS and WE transects it is shown that rainfall is observed more frequently on the windward side of the high mountain ranges of Choke-mountain than on the leeward side. Also mean rain rates generally are higher on the windward side and lower on the leeward side of the north and north-east facing hill slopes. This indicates that the general pattern of air circulation is obstructed by the Choke-mountain range resulting in specific local rainfall characteristics. The rainfall pattern also is affected by the deep and wide Blue Nile River gorge with relatively low rainfall occurrence and low mean rainfall depth in the gorge area. For the centre of the basin where the gorge is deepest and widest, and on the left bank areas that are east and north-east of the gorge relatively high occurrence and rain rates are observed. Results of both PR and TMI show relatively large variability of rainfall rates and occurrence in the Lake Tana basin area. Rainfall is most frequent during night hours with higher mean rainfall depth on the south shore than on the north shore.

The diurnal cycle patterns from PR and TMI are compared to ground observations from three recording stations that have different diurnal cycle characteristics. In general, the pattern of the diurnal cycle of rainfall occurrence from PR and TMI estimations matches with the ground truth although some very large differences are shown for LSTs with high occurrence. Results show that rainfall occurrence from TMI in general is higher than PR but also that for most of the LSTs the ground observation have lowest occurrence. A correlation analysis between the satellite estimates and ground observations shows that the diurnal cycle of both rainfall occurrence and rain rate from PR estimations is closer to the ground observations than TMI. A comparison against ground observations shows that satellite estimates are more suited to assess rainfall occurrence than rain rate.

Analysis on the spatial distribution of the estimated wet seasonal rainfall depth indicates large variability over the basin. The areas in the south-west and central highlands of the basin receive higher amounts of rainfall than the areas in the north and north-east parts of the basin. Along the main stream of the Blue Nile River and particularly for PR a distinct pattern is shown with a low amount of rainfall. The PR estimated seasonal rainfall depth is closer to the ground observations than the TMI estimate. The TMI estimated rainfall depth at Shawura which is located at 9 km from Lake Tana is nearly 2 times larger than the ground truth and PR. To verify the satellite estimated daily mean rainfall depth time series of 9 collector stations in the basin are used. Results show that PR estimates are lower than gauge estimates whereas TMI often shows higher values than gauges. Differences between the PR and TMI estimates are not very consistent. In this study we did not evaluate specific causes of estimation uncertainty that relate to limitations and constrains of the retrieval algorithms. We exclusively aimed at using the TRMM PR and TMI satellite rainfall products to assess specific aspects of rainfall variability across the UBN area including effects of large scale topographic features.

References

Abdo, K.S., Fiseha, B.M., Rientjes, T.H.M., Gieske, A.S.M., Haile, A.T., 2009. Assessment of climate change impacts on the hydrology of Gilgel Abay catchment in Lake Tana basin, Ethiopia. Hydrological Processes 23 (6), 3661–3669.

Abtew, W., Melesse, A.M., Dessalegne, T., 2008. Characteristics of monthly and annual rainfall of the Upper Blue Nile basin. In: Abtew, W., Melesse, A.M. (Eds.), Proceedings of the Workshop on Hydrology and Ecology of the Nile River Basin under Extreme Conditions,. Addis Ababa, Ethiopia, June 16–19, 2008.

Arora, M., Singh, P., Goel, N.K., Singh, R.D., 2006. Spatial distribution and seasonal variability of rainfall in a mountainous basin in the Himalayan region. Water Resources Management 20, 489–508.

Barros, A.P., Kim, G., Williams, E., Nesbitt, S.W., 2004. Probing orographic controls in the Himalayas during the monsoon using satellite imagery. Natural Hazards and Earth System Sciences 4 (1), 29–51.

Bell, T.L., Reid, N., 1993. Detecting the diurnal cycle of rainfall using satellite observations. Journal of Applied Meteorology 32 (2), 311–322.

Bowman, K.P., Collier, J.C., North, G.R., Wu, Q., Ha, E., 2005. Diurnal cycle of tropical precipitation in Tropical Rainfall Measuring Mission (TRMM) satellite and ocean buoy rain gauge data. Journal of Geophysical Research 110, D21104, http://dx.doi.org/10.1029/2005JD005763.

Camberlin, P., 1997. Rainfall anomalies in the source region of the Nile and their connection with the Indian summer monsoon. Journal of Climate 10 (6), 1380–1392.

Camberlin, P., 2009. Nile basin climates. In: Dumont, H.J. (Ed.), The Nile: Origin, Environments, Limnology and Human Use. Monographiiae Biologicae. Springer, pp. 307–333.

Conway, D., 2000. The climate and hydrology of the Upper Blue Nile, Ethiopia. The Geographical Journal 166 (1), 49–62.

Deckers, D.L.E.H., Booij, M.J., Rientjes, T.H.M., Krol, M.S., 2010. Catchment variability and parameter estimation in multi – objective regionalisation of a rainfall – runoff model. In: Water resources management, http://dx.doi.org/10.1007/s11269-010-9642-8

de Vos, N.J., Rientjes, T.H.M., 2008. Multi-objective training of artificial neural networks for rainfall-runoff modeling. Water Resources Research 44 (2008), W08434.

de Vos, N.J., Rientjes, T.H.M., Gupta, H.V., 2010. Diagnostic evaluation of conceptual rainfall-runoff models using temporal clustering. Hydrological Processes, http://dx.doi.org/10.1002/hyp.7698.

Fenicia, F., Zhang, G.P., Rientjes, T.H.M., Hoffmann, L., Pfister, L., Savenije, H.H.G., 2005. Numerical simulations of runoff generation with surface water–groundwater interaction in the Alzette river alluvial plain, Luxembourg. Physics and Chemistry of the Earth 30 (4–5), 277–284.

Furuzawa, F.A., Nakamura, K., 2005. Differences of rainfall estimates over land by Tropical Rainfall Measuring Mission (TRMM) Precipitation Radar (PR) and TRMM Microwave Imager (TMI)-Dependence on Storm Height. Journal of Applied Meteorology 44 (3), 367–383.

Haile, A.T., Habib, E., Rientjes, T.H.M., 2012a. Evaluation of the climate prediction center (CPC) morphing technique (CMORPH) rainfall product on hourly time scales over the source of the Blue Nile River. Hydrological Processes, http://dx.doi.org/10.1002/hyp.9330.

Haile, A.T., Habib, E., Elsaadani, M., Rientjes, T.H.M., 2012b. Inter-comparison of satellite rainfall products for representing rainfall diurnal cycle over the Nile basin. International Journal of Applied Earth Observation and Geoinformation, http://dx.doi.org/10.1016/j.jag.2012.08.012

Haile, A.T., Rientjes, T.H.M., Gieske, A.S.M., 2009. Rainfall variability over mountainous and adjacent lake areas: the case of Lake Tana basin at the source of the Blue Nile river. Journal of Applied Meteorology and Climatology 48 (8), 1696–1717.

Haile, A.T., Rientjes, T.H.M., Gieske, A.S.M., Mekonnen, G., 2010. Multispectral remote sensing for rainfall detection and estimation at the source of the Blue Nile River. International Journal of Applied Earth Observation and Geoinformation 12 (Suppl. 1), S76–S82.

Haile, A.T., Rientjes, T.H.M., Habib, E., Jetten, V., Gebremichael, M., 2011. Rain event properties at the source of the Blue Nile River. Hydrology and Earth System Sciences 15, 1023–1034, http://dx.doi.org/10.5194/hess-15-1023-2011, www.hydrol-earth-syst-sci.net/15/1023/2011

Hirose, M., Oki, R., Shimizu, S., Kachi, M., Higashiuwatoko, T., 2008. Fine scale diurnal rainfall statistics refined from eight years of TRMM PR data. Journal of Applied Meteorology and Climatology 47, 544–561.

Iguchi, T., Kozu, T., Meneghini, R., Awaka, J., Okamoto, K., 2000. Rain-profiling algorithm for the TRMM Precipitation Radar. Journal of Applied Meteorology 39 (12), 2038–2052.

Ikai, J., Nakamura, K., 2003. Comparison of Rain rates over the ocean derived from TRMM Microwave Imager and Precipitation Radar. Journal of Atmospheric and Oceanic Technology 20 (12), 1709–1726.

Ji, Y., 2006. Validation of diurnal cycle and intra-seasonal variability of TRMM satellite rainfall. PIERS ONLINE 2 (6), 628–632.

Kim, U., Kaluarachchi, J.J., 2008. Application of parameter estimation and regionalization methodologies to ungauged basins of the Upper Blue Nile River Basin, Ethiopia. Journal of Hydrology 362 (1–2), 39–56.

Kim, U., Kaluarachchi, J.J., Smakhtin, V.U., 2008. Generation of Monthly precipitation under climate change for the Upper Blue Nile River Basin, Ethiopia. Journal of the American Water Resources Association 44 (5), 1231–1247.

Kishtawal, C.M., Krishnamurti, T.N., 2001. Diurnal variation of summer rainfall over Taiwan and its detection using TRMM observations. Journal of Applied Meteorology 40 (3), 331–344.

Kummerow, C., Barnes, W., Kozu, T., Shiue, J., Simpson, J., 1998. The Tropical Rainfall Measuring Mission (TRMM) sensor package. Journal of Atmospheric and Oceanic Technology 15 (3), 809–817.

Kummerow, C., Simpson, J., Thiele, O., Barnes, W., Chang, A.T.C., Stocker, E., Adler, R.F., Hou, A., Kakar, R., Wentz, F., Ashcroft, P., Kozu, T., Hong, Y., Okamoto, K., Iguchi, T., Kuroiwa, H., Im, E., Haddad, Z., Huffman, G., Ferrier, B., Olson, W.S., Zipser, E., Smith, E.A., Wilheit, T.T., North, G., Krishnamurti, T., Nakamura, K., 2000. The status of the Tropical Rainfall Measuring Mission (TRMM) after two years in orbit. Journal of Applied Meteorology 39 (12), 1965–1982.

Kuraji, K., Punyatrong, K., Suzuki, M., 2001. Altitudinal increase in rainfall in the Mae Chaem watershed, Thailand. Journal of the Meteorological Society of Japan 79 (1B), 353–363.

Meneghini, R., Iguchi, T., Kozu, T., Liao, L., Okamoto, K., Jones, J.A., Kwiatkowski, J., 2000. Use of the surface reference technique for path attenuation estimates from the TRMM precipitation radar. Journal of Applied Meteorology 39, 2053–2070.

Muthuwatta, L.P., Ahmad, M.D., Bos, M.G., Rientjes, T.H.M., 2010. Assessment of water availability and consumption in the Karkheh River basin, Iran: using remote sensing and geo-statistics. Water Resources Management 24 (3), 459–484.

Negri, A.J., Bell, T.L., Xu, L., 2002. Sampling of the diurnal cycle of precipitation using TRMM. Journal of Atmospheric and Oceanic Technology 19 (9), 1333–1344.

Nesbitt, S.W., Zipser, E.J., Kummerow, C.D., 2004. An examination of version-5 rainfall estimates from the TRMM Microwave Imager, Precipitation Radar, and Rain Gauges on Global, Regional, and Storm Scales. Journal of Applied Meteorology 43 (7), 1016–1036.

Rientjes, T.H.M., Alemseged, T.H., Kebede, E., Mannaerts, C., Habib, E., Steenhuis, T.S., 2011a. Changes in land cover and stream flow in Gilgel Abay watershed, Blue Nile Basin Ethiopia. Hydrology and Earth System Sciences 15, 1979–1989, http://dx.doi.org/10.5194/hess-15-1979-2011.

Rientjes, T.H.M., Perera, B.U.J., Haile, A.T., Reggiani, P., Muthuwatta, L.P., 2011b. Regionalisation for lake level simulation – the case of Lake Tana in the Upper Blue Nile, Ethiopia. Hydrology and Earth System Sciences 15, 1167–1183, http://dx.doi.org/10.5194/hess-15-1167-2011, www.hydrol-earth-syst-sci.net/15/1167/2011

Sapiano, M.R.P., Arkin, P.A., 2009. An intercomparison and validation of high-resolution satellite precipitation estimates with 3-hourly gauge data. Journal of Hydrometeorology 10, 149–166.

Simpson, J., Adler, R.F., North, G.R., 1988. A proposed tropical Rainfall Measuring Mission (TRMM) Satellite. Bulletin of the American Meteorological Society 69 (3), 278–295.

Sutcliffe, J.V., Parks, Y.P., 1999. The Hydrology of the Nile, IAHS Special Publication No. 5. IAHS Press, Institute of Hydrology, Wallingford, Oxford Shine.

Tarekegn, H.T., Haile, A.H., Rientjes, T.H.M., Reggiani, P., Alkema, D., 2010. Assessment of an ASTER-generated DEM for 2D-hydrodynamic flood modeling, International Journal of Applied Earth Observation and Geoinformation, http://dx.doi.org/10.1016/j.jag.2010.05.007

UNESCO, 2004. National Water Development Report for Ethiopia. UN-WATER/WWAP/2006/7, World Water Assessment Program Report, MOWR: 284.

Wale, A., Rientjes, T.H.M., Gieske, A.S.M., Getachew, H.A., 2009. Ungauged catchment contributions to Lake Tana's water balance. Hydrological Processes 23 (26), 3682–3693.

Yamamoto, M.K., Furuzawa, F.A., Huguchi, A., Nakamura, K., 2008. Comparison of diurnal variations in precipitation systems observed by TRMM PR, TMI, and VIRS. Journal of Climate 21, 4011–4028.

Zhang, G.P., Fenicia, F., Rientjes, T.H.M., Reggiani, P., Savenije, H.H.G., 2005. Modeling runoff generation in the Geer river basin with improved model parameterizations to the REW approach. Physics and Chemistry of the Earth 30 (4–5), 285–296, http://dx.doi.org/10.1016/j.pce.2004.11.002.